JOURNAL OF COMPUTATIONAL PHYSICS 47, 130–145 (1982)

A Numerical Study of Wind-Driven Circulation in Rectangular Cavities

MICHIO KUMAGAI*

Department of Oceanography, University of Southampton, England

Received July 14, 1981; revised December 1, 1981.

The improved ADI method is used to solve the problem of wind-driven circulation in a rectangular cavity, and it is shown that the rate of convergence is not strongly dependent on the Reynolds number or the size of the mesh. Steady state solutions of vorticity and stream function are computed for four different values of the aspect ratio, and the results are described. Vertical profiles of horizontal velocity and its vertical curvature are also presented. Notable features of the results are the existence of physical differences between large and small aspect ratios and the suggestion of a *symptom of transition* from laminar to turbulent flow.

1. INTRODUCTION

Although the problem of wind-driven circulation in rectangular cavities is basic to the estimation of the energy transfer from wind to water, few works are to be found on this subject. The study of circulation induced by a constant shear stress at the water surface was theoretically presented by Hidaka [1] and numerically considered by Bye [2]. Bye discussed the behavior of the flow at both the upwind and the downwind ends, and showed the hydrodynamic instability of the stream lines at Reynolds numbers between 400 and 600, as he defined them. Furthermore, the problem of circulation in a rectangular cavity, induced by a parallel shear flow, was studied by Weiss and Florsheim [3], O'Brien [4], and Brandeis and Rom [5]. It is true that their line of approach is suitable for the problem of wind-driven circulation, but it is still difficult to use the appropriate matching method at the water surface.

On the other hand, Kawaguchi [6] examined numerically the cavity flow problem in which the circulation was induced by a surface wall moving at a constant speed. After his work, a number of investigations of this type were made, and some of them were reviewed by Tuann and Olson [7]. The numerical techniques developed for the cavity flow problem are suitable for the problem of wind-driven circulation because the governing equations are of a similar type, except for the surface boundary conditions.

The purpose of this paper is to solve numerically the steady state problem of wind-driven circulation originally proposed by Hidaka [1] using the improved ADI

* Present address: Department of Geophysics, Kyoto University, Sakyoku, Kyoto 606, Japan.

0021-9991/82/070130-16$02.00/0

method. The numerical simulation of circulation induced by a constant vorticity at the water surface is employed. Note that this model is slightly different from the ordinal cavity model mentioned above. Of special concern is examining how the pattern of circulation in rectangular cavities changes with Reynolds number and aspect ratio.

2. Mathematical Formulation of Wind-Driven Circulation

Let us consider a two-dimensional rectangular cavity of height H and width L, in which water of constant density ρ and viscosity μ is set into motion by a steady homogeneous wind blowing over the water surface. The x-axis is taken along the bottom of the cavity and the y-axis vertically, the origin being taken at the bottom left-hand corner as shown in Fig. 1. After a sufficient time, the flow of water in the cavity should reach a steady state balance with constant tangential wind stress at the water surface. Since without wind there exists no flow of water in the cavity, this circulation must be characterized by the friction velocity, u_*, of air.

Now let the governing equations be dimensionless with the horizontal length L and the friction velocity u_*; then,

$$J(\psi, \zeta) = (1/\mathrm{Re})\,\nabla^2\zeta, \tag{1}$$

$$\nabla^2\psi = -\zeta, \tag{2}$$

$$\psi = 0 \qquad \text{along all boundaries,} \tag{3}$$

$$\frac{\partial\psi}{\partial x} = 0 \qquad \text{along vertical walls,} \tag{4}$$

$$\frac{\partial\psi}{\partial y} = 0 \qquad \text{along a bottom wall,} \tag{5}$$

$$\zeta = (\rho_a/\rho)\,\mathrm{Re} \qquad \text{along a water surface,} \tag{6}$$

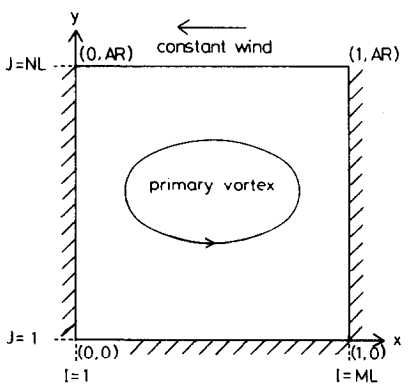

FIG. 1. Schematic sketch of the rectangular cavity.

where J is the Jacobian, $\nabla^2 = (\partial^2/\partial x^2) + (\partial^2/\partial y^2)$; ψ is the stream function; ζ is the vorticity, ρ_a is the density of air, and Re is the Reynolds number defined as

$$\mathrm{Re} = \rho u_* L/\mu. \tag{7}$$

Using the surface velocity u_s at the midpoint of the cavity, Re can be connected with Reynolds number Re^B defined by Bye [2] as

$$\mathrm{Re}^B = \rho u_s H/\mu = \mathrm{AR}(u_s/u_*)\,\mathrm{Re}, \tag{8}$$

and AR is the aspect ratio defined as,

$$\mathrm{AR} = H/L, \tag{9}$$

where L is the horizontal scale of the cavity and H the vertical one.

As we are concerned with just a steady state solution, Eqs. (1) and (2) may be rewritten as a Cauchy–Kovaleska equation, i.e.,

$$\frac{\partial \zeta}{\partial t} = \varepsilon \left[-J(\psi, \zeta) + \frac{1}{\mathrm{Re}} \nabla^2 \zeta \right], \tag{10}$$

$$\frac{\partial U}{\partial t} = -\varepsilon[\nabla^2 \psi + \zeta], \tag{11}$$

wwhere ε is a parameter used to enhance the transient convergence.

3. Finite Difference Equations

In order to construct finite difference analogues of Eqs. (10) and (11), the ADI method originally proposed by Peaceman and Rachford [8] is used herein. According to Pearson [9], Eqs. (10) and (11) may be approximated by

$$\begin{aligned}\frac{\zeta_{i,j}^{n+1/2} - \zeta_{i,j}^{n}}{\Delta t/2} = \varepsilon_n \Bigg\{ & \frac{1}{\mathrm{Re}} \left[\frac{\zeta_{i+1,j}^{n+1/2} + \zeta_{i-1,j}^{n+1/2} - 2\zeta_{i,j}^{n+1/2}}{(\Delta x)^2} + \frac{\zeta_{i,j+1}^{n} + \zeta_{i,j-1}^{n} - 2\zeta_{i,j}^{n}}{(\Delta y)^2} \right] \\ & + (1/4\Delta x\,\Delta y)(\zeta_{i,j+1}^{n} - \zeta_{i,j-1}^{n})(\psi_{i+1,j}^{n} - \psi_{i-1,j}^{n}) \\ & - (1/4\Delta x\,\Delta y)(\zeta_{i+1,j}^{n+1/2} - \zeta_{i-1,j}^{n+1/2})(\psi_{i,j+1}^{n} - \psi_{i,j-1}^{n}) \Bigg\}, \end{aligned} \tag{12}$$

$$\begin{aligned}\frac{\zeta_{i,j}^{n+1} - \zeta_{i,j}^{n+1/2}}{\Delta t/2} = \varepsilon_n \Bigg\{ & \frac{1}{\mathrm{Re}} \left[\frac{\zeta_{i+1,j}^{n+1/2} + \zeta_{i-1,j}^{n+1/2} - 2\zeta_{i,j}^{n+1/2}}{(\Delta x)^2} + \frac{\zeta_{i,j+1}^{n+1} + \zeta_{i,j-1}^{n+1} - 2\zeta_{i,j}^{n+1}}{(\Delta y)^2} \right] \\ & + (1/4\Delta x\,\Delta y)(\zeta_{i,j+1}^{n+1} - \zeta_{i,j-1}^{n+1})(\psi_{i+1,j}^{n} - \psi_{i-1,j}^{n}) \\ & - (1/4\Delta x\,\Delta y)(\zeta_{i+1,j}^{n+1/2} - \zeta_{i-1,j}^{n+1/2})(\psi_{i,j+1}^{n} - \psi_{i,j-1}^{n}) \Bigg\}, \end{aligned} \tag{13}$$

$$\frac{\psi_{i,j}^{n+1/2}-\psi_{i,j}^{n}}{\Delta t/2}=-\varepsilon_n\left[\frac{\psi_{i+1,j}^{n+1/2}+\psi_{i-1,j}^{n+1/2}-2\psi_{i,j}^{n+1/2}}{(\Delta x)^2}+\frac{\psi_{i,j+1}^{n}+\psi_{i,j-1}^{n}-2\psi_{i,j}^{n}}{(\Delta y)^2}+\zeta_{i,j}^{n+1}\right], \tag{14}$$

$$\frac{\psi_{i,j}^{n+1}-\psi_{i,j}^{n+1/2}}{\Delta t/2}=-\varepsilon\left[\frac{\psi_{i+1,j}^{n+1/2}+\psi_{i-1,j}^{n+1/2}-2\psi_{i,j}^{n+1/2}}{(\Delta x)^2}+\frac{\psi_{i,j+1}^{n+1}+\psi_{i,j-1}^{n+1}-2\psi_{i,j}^{n+1}}{(\Delta y)^2}+\zeta_{i,j}^{n+1}\right]. \tag{15}$$

Eq. (12) can be rewritten as,

$$-A_{ij}^{n}\zeta_{i+1,j}^{n+1/2}+B^{n}\zeta_{i,j}^{n+1/2}-C_{ij}^{n}\zeta_{i-1,j}^{n+1/2}=D_{ij}^{n}, \tag{16}$$

where

$$A_{ij}^{n}=(1/\mathrm{Re}(\Delta x)^2)-(1/4\Delta x\,\Delta y)(\psi_{i,j+1}^{n}-\psi_{i,j-1}^{n}),$$

$$B^{n}=2/\varepsilon_n\Delta t+2/\mathrm{Re}(\Delta x)^2,$$

$$C_{ij}^{n}=(1/\mathrm{Re}(\Delta x)^2)+(1/4\Delta x\,\Delta y)(\psi_{i,j+1}^{n}-\psi_{i,j-1}^{n}),$$

$$D_{ij}^{n}=[(1/\mathrm{Re}(\Delta y)^2)+(1/4\Delta x\,\Delta y)(\psi_{i+1,j}^{n}-\psi_{i-1,j}^{n})]\,\zeta_{i,j+1}^{n}+[(1/\mathrm{Re}(\Delta y)^2)-(1/4\Delta x\,\Delta y)(\psi_{i+1,j}^{n}-\psi_{i-1,j}^{n})]\,\zeta_{i,j-1}^{n}+\left[\frac{2}{\varepsilon_n\Delta t}-\frac{2}{\mathrm{Re}(\Delta y)^2}\right]\zeta_{i,j}^{n}.$$

Equations (13)–(15) may also be reduced to the same form as Eq. (16). A way to solve equations of this type can be seen in Roache [10].

The boundary conditions of Eqs. (3)–(6) are discretized to the second order, say,

$$\psi_{1,j}=\psi_{ML,j}=\psi_{i,1}=\psi_{i,NL}=0, \tag{17}$$

$$\zeta_{1,j}=(3\psi_{2,j}/(\Delta x)^2)-\tfrac{1}{2}\zeta_{2,j}, \tag{18}$$

$$\zeta_{\mathrm{ML},j}=(3\psi_{\mathrm{ML}-1,j}/(\Delta x)^2)-\tfrac{1}{2}\zeta_{\mathrm{ML}-1,j}, \tag{19}$$

$$\zeta_{i,1}=(3\psi_{i,2}/(\Delta y)^2)-\tfrac{1}{2}\zeta_{i,2}, \tag{20}$$

$$\zeta_{i,\mathrm{NL}}=(\rho_a/\rho)\,\mathrm{Re}, \tag{21}$$

where ML and NL correspond to the numbers of horizontal and vertical mesh points as shown in Fig. 1.

In Eqs. (12)–(15), the parameter ε_n can be changed every iteration, because the ADI method is unconditionally stable at any time step. As stated by Roache [10], it

is not easy to determine an optimum parameter of ε_n, so we use the method introduced by Miyakoda [11], say,

$$P_n = 2/\Delta t\varepsilon_n = YX^{n-1}, \tag{22}$$

where X and Y are the arbitrary values restricted by $0 < X \leqslant 1$ and $0 < Y$, and those values used in this computation are tabulated in Table I.

As the number of iterations increases, however, P_n diminishes, and there is a possibility that the iteration may be terminated before the following criterion of convergence is satisfied:

$$|(f^n - f^{n-1})/f^n_{\max}|_{\max} < 10^{-6}, \tag{23}$$

where f represents either vorticity ζ or stream function ψ. To avoid this possibility, we introduce a second criterion,

$$P_n > 10^{-4}. \tag{24}$$

This means that the time step changes within the limited interval. If P_n becomes less than 10^{-4}, P_n reverts back to P_1, and the iteration is then repeated. Birkhoff *et al.* [12] showed that if the repetition of the iteration parameters is used, the number

TABLE I

Numerical Conditions

Aspect ratio	Reynolds number		Iteration parameters[a]	
AR	Re	Re^B	X	Y
1.0	100	1.735	0.5	1.0
	400	26.68	0.5	1.0
	1000	112.9	0.5	1.0
	2000	300.0	0.5	1.0
0.5	100	0.711	0.5	1.0
	400	11.12	0.5	1.0
	1000	52.20	0.5	1.0
	2000	135.8	0.8	1.0
0.1	100	0.033	0.5	1.0
	1000	3.249	0.5	1.0
	2000	13.00	0.5	1.0
	4500	60.12	0.5	1.0
0.05	100	0.001	0.5	1.0
	1000	0.809	0.5	1.0
	5000	20.27	0.5	1.0
	10000	76.15	0.5	1.0

[a] See Eq. (22).

of iterations does not strongly depend on the size of the mesh. The combination of the criteria represented by Eqs. (23) and (24) is the improved point of this numerical model.

The finite difference equations, including the boundary conditions, used in this paper all have second-order accuracy. We sometimes fail, however, to obtain the convergence because of the nonlinearity of Eqs. (12) and (13). This problem may be resolved by changing the combination of the values of X and Y in Eq. (22). The numerical conditions used herein are tabulated in Table I.

Now let us list the steps in the computational procedure.

(1) Assume that the initial values of ζ and ψ at the required mesh point are zero.

(2) Set boundary values of ζ and ψ with Eqs. (17)–(21).

(3) Solve Eqs. (12) and (13) to give ζ^{n+1}.

(4) Using the values of ζ^{n+1}, solve Eqs. (14) and (15) to give ψ^{n+1}.

(5) Repeat step (2) iteratively until the convergence criterion of Eq. (23) is satisfied for both ζ and ψ.

(6) Calculate horizontal velocity with the following equation:

$$u_{i,j} = (\psi_{i,j+1} - \psi_{i,j-1})/2\Delta y \qquad \text{for} \quad j = 2, \text{NL} - 1,$$

$$u_{i,1} = 0.$$

The surface horizontal velocity is estimated as follows:

$$u_{i,\text{NL}} = -\psi_{i,\text{NL}-1}/\Delta y + (\Delta y/3)(\zeta_{i,\text{NL}} + \tfrac{1}{2}\zeta_{i,\text{NL}-1}).$$

All these are also correct to the second order in Δy. All calculations are carried out on a 41×41 mesh, and P_n is changed at each iteration under the restriction of Eq. (24).

4. Numerical Results and Discussion

With a constant vorticity source at the water surface as shown in Fig. 1, a counter-clockwise vortex is induced in the rectangular cavity as shown in Fig. 2. Note that all cases are shown to the same scale, regardless of the different aspect ratios used.

The most notable feature of the ADI method compared with the SOR method (for example, Takematsu [13]) is that the number of iterations for convergence only increases slowly as the Reynolds number is increased, as seen in Fig. 2. All results demonstrated herein are obtained on a 41×41 mesh, but we also tried a few cases for AR = 1.0 on a 21×21 mesh in order to examine the dependence of the rate of convergence on the mesh size for this numerical method. These results are shown in Table II, and it is found that the rate of convergence of the ADI method is not strongly influenced by the size of the mesh.

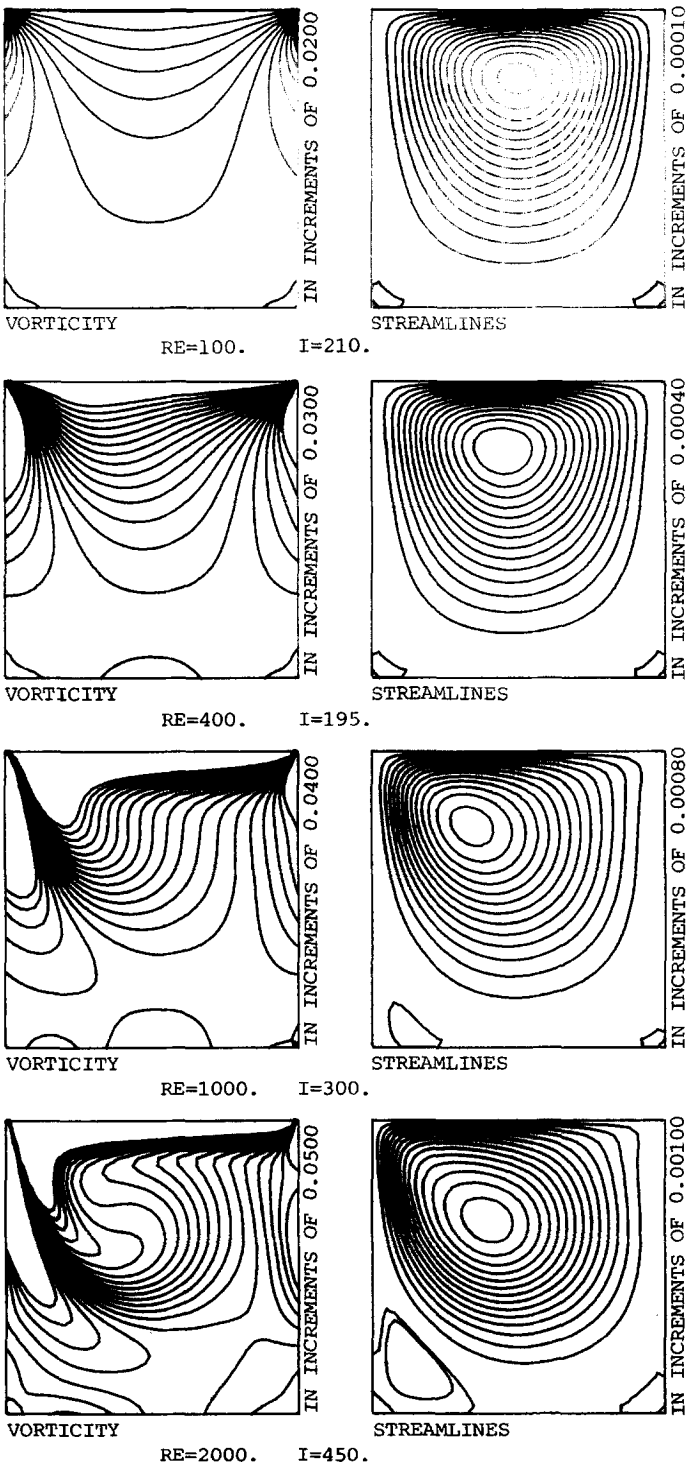

FIG. 2(a) Vorticity and stream function fields for AR = 1.0. The inner contour of secondary eddy is drawn at $\psi = -0.00005$. $DX = 0.025$; $DY = 0.02500$.

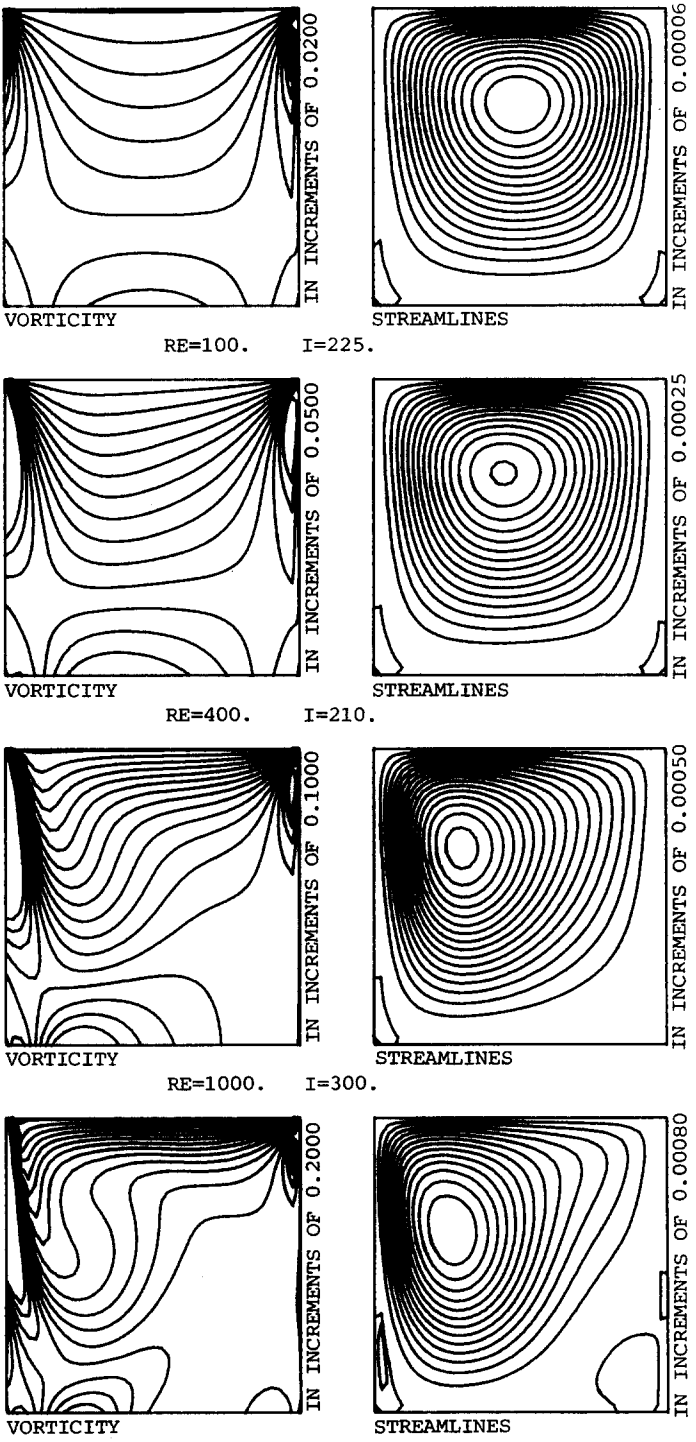

FIG. 2(b) Vorticity and stream function fields for AR = 0.5. The inner contour of secondary eddy is drawn at $\psi = -0.00005$. $DX = 0.025$; $DY = 0.01250$.

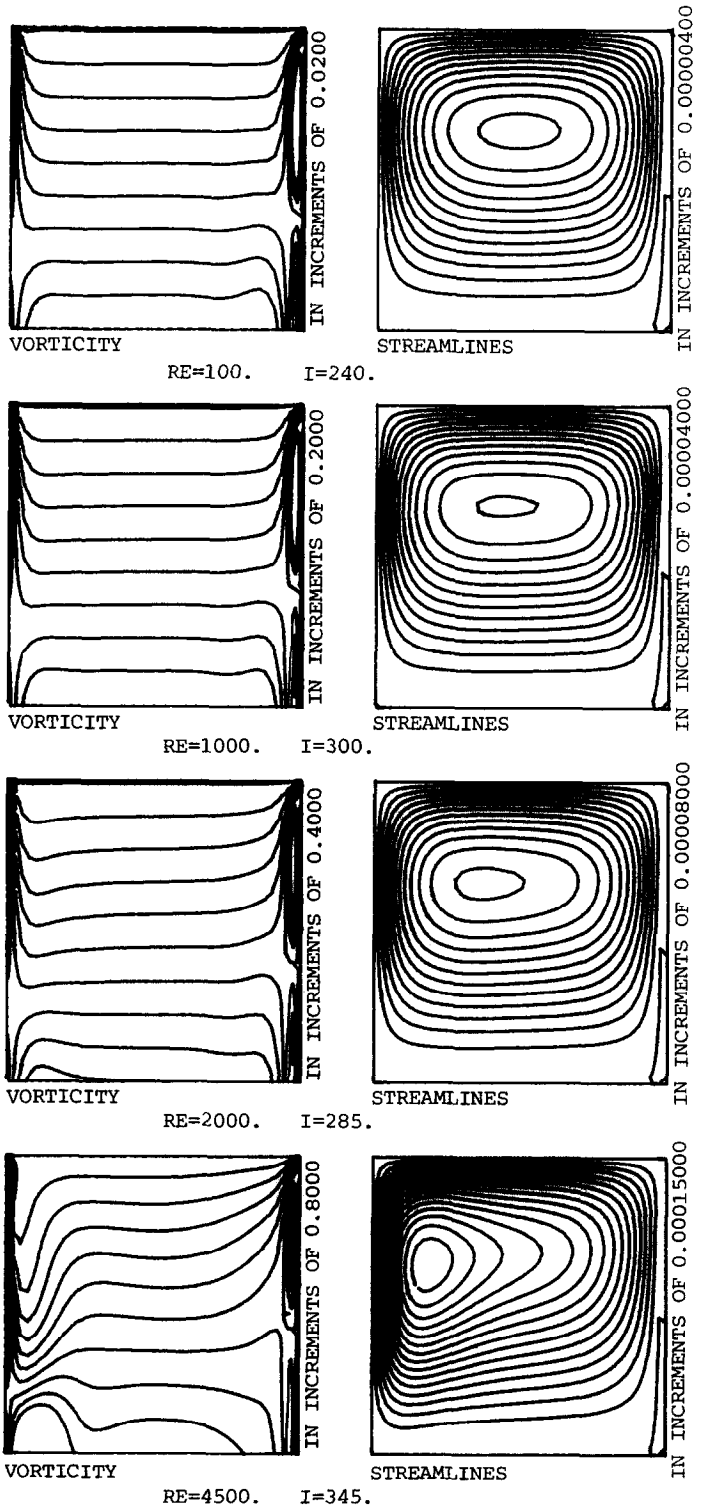

FIG. 2(c) Vorticity and stream functions fields for AR = 0.1. $DX = 0.025$; $DY = 0.00250$.

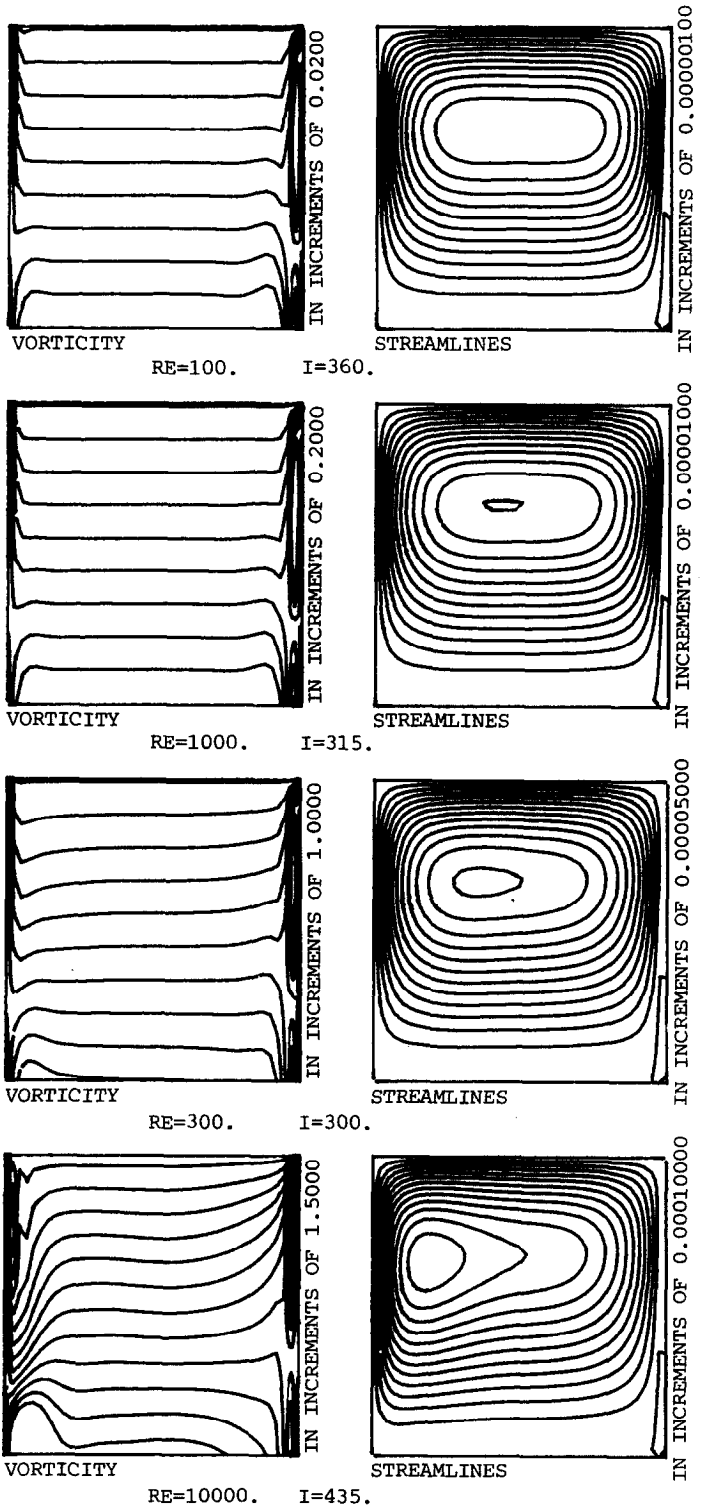

FIG. 2(d) Vorticity and stream function fields for AE = 0.05. $DX = 0.025$; $DY = 0.00125$.

TABLE II

Dependence of the Rate of Convergence on the Mesh Size at AR = 1.0

Reynolds number Re	Number of iterations	
	21 × 21 mesh	41 × 41 mesh
100	135	210
400	150	195
1000	270	300

Now let us discuss the numerical results. First of all, it is readily found from Figs. 2a–d that the contours of vorticity become asymmetrical as the Reynolds number is increased. The same tendency can be seen in the contours of stream lines. The behavior of vorticity and stream lines at AR = 1.0 in Fig. 2a is very similar to that of the cavity problem discussed by Burggraf [14]. The circulation tends to close to the downwind end of the cavity as the Reynolds number is increased. This means that the inertia terms are becoming more dominant. This effect was originally studied by Hidaka [1].

Next, as shown in Figs. 2a and b, for both AR = 1.0 and AR = 0.5, it is found that there exist secondary eddies at both the bottom corners, except for the case of Re = 1000 at AR = 0.5. Although it is difficult to explain the reason for this exception at AR = 0.5, the general tendency seems to be consistent with the results on the cavity flow problem. On the other hand, from Figs. 2c and d, only one secondary eddy can be seen, at the bottom right-hand corner, in the cases of AR = 0.1 and AR = 0.05. These facts imply that there is a physical difference between the case of AR = 1.0 and AR = 0.5 and the case of AR = 0.1 or AR = 0.05.

Third, it should be noted that the Reynolds number increases as the aspect ratio decreases. For example, although the maximum Reynolds number at AR = 1.0 is 2000 in Fig. 2a, it is 10,000 at AR = 0.05, as seen in Fig. 2d. This means that wind-driven circulation tends to be more stable at a small aspect ratio than at a large one. In other words, a smaller aspect ratio requires a larger Reynolds number to obtain the same order of velocity. This discussion of a larger aspect ratio than AR = 1.0 was presented by O'Brien [4].

Fourth, according to the experimental results of Keulegan [15], a transition from laminar to turbulent flow may happen between Re^B values of 400 and 1000. These values are much less than those of the cavity flow problem experimentally reported by Mills [16] and Pan and Acrivos [17]. This fact shows that wind-driven circulation become unstable at a rather smaller Reynolds number than does the

FIG. 3 The vertical profiles of horizontal velocity $u_{i,j}$ for AR = 1.0 and AR = 0.5.

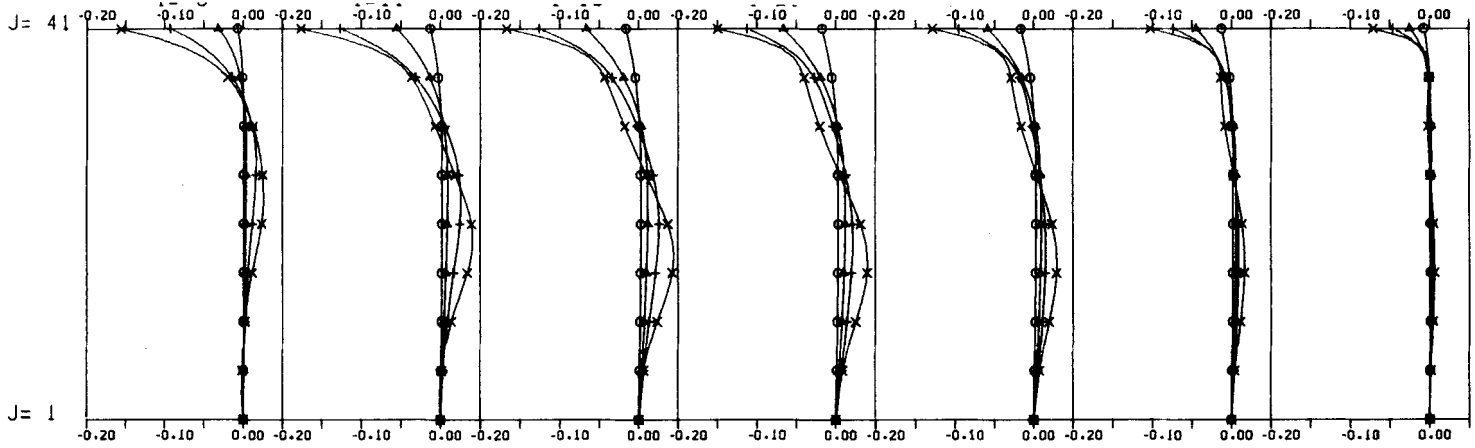

AR= 1.000 :⊙ RE=100. :△ RE=400. :+ RE=1000. :× RE=2000.

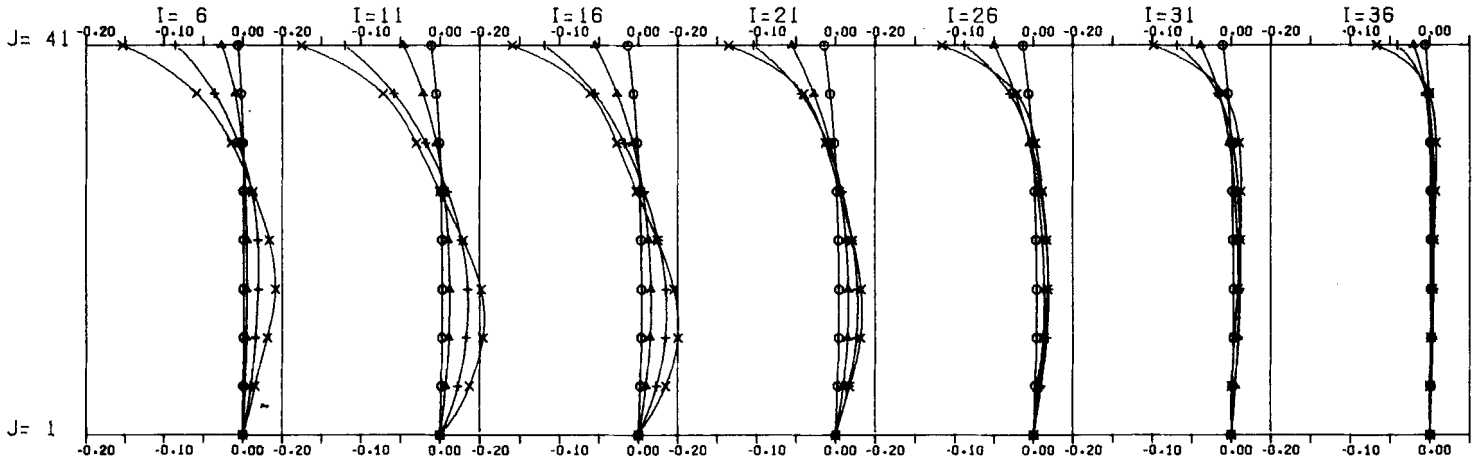

AR= 0.500 :⊙ RE=100. :△ RE=400. :+ RE=1000. :× RE=2000.

cavity flow problem. Bye [2] demonstrated numerically that the transition from laminar to turbulent flow happens between Re^B values of 400 and 600. In fact, it is very difficult to predict the transient Reynolds number from laminar to turbulent flow in a numerical method for the steady-state problem. Approaching the transitional state, the numerical solutions may oscillate as mentioned by Bye [2]. The vertical profiles of horizontal velocity for AR = 1.0 and AR = 0.5 are shown in Fig. 3. It is found that the profiles for Re = 2000 at both aspect ratios (which are indicated by $\times$) are slightly bent. As seen in Table I, these Reynolds numbers correspond to $Re^B = 300$ and $Re^B = 135.8$, respectively. If this kind of variation has some connection with transition from laminar to turbulent flow, it may appear at a Reynolds number rather lower than the value mentioned above. We have, however, little conviction regarding this symptom. It should be certified by wind-tunnel experiments in the future. A similar tendency is observed to occur in a cavity flow problem (for example, Leonard [18]).

Lastly, the vertical curvature of horizontal velocity for AR = 1.0 and AR = 0.5 is plotted in Fig. 4, where the curvature is calculated as follows:

$$u''_{i,j} = (u_{i,j+1} + u_{i,j-1} - 2u_{i,j})/(\Delta y)^2. \tag{25}$$

Using Eq. (25), the values of the curvature at the bottom and top of the cavity are not obtainable. Consider just a line of $I = 21$, where the influence of vertical velocity is less. The profile of curvature can be divided into two regions, the upper region of large value of curvature and the lower region of nearly constant value of curvature. In the upper region, it should be noted that the curvature decreases sharply at Reynolds numbers under Re = 1000 very near the water surface. This may indicate the existence of a viscous surface sub-layer, because the vertical profile of horizontal velocity is linear with depth and the curvature is zero in the viscous sub-layer. As the Reynolds number is increased, the viscous sub-layer disappears and the profile of curvature becomes continuous near the water surface as the result of the nonlinearity seen in Re = 2000 at AR = 1.0. This fact may be connected with the variation of the vertical profile of horizontal velocity. In the lower region, the vertical profiles of curvature seem to be constant. They look to be zero but are not exactly zero. This means that the vertical profiles of horizontal velocity in this region are close to being parabolic.

5. Conclusion

Let us summarize the results discussed in the previous section.

1. The improved ADI method in this paper has a good rate of convergence to a steady state solution. This rate of convergence is not strongly dependent on the Reynolds number of the size of the mesh.

FIG. 4 The vertical profiles of the curvature of horizontal velocity $u''_{i,j}$ for AR = 1.0 and AR = 0.5.

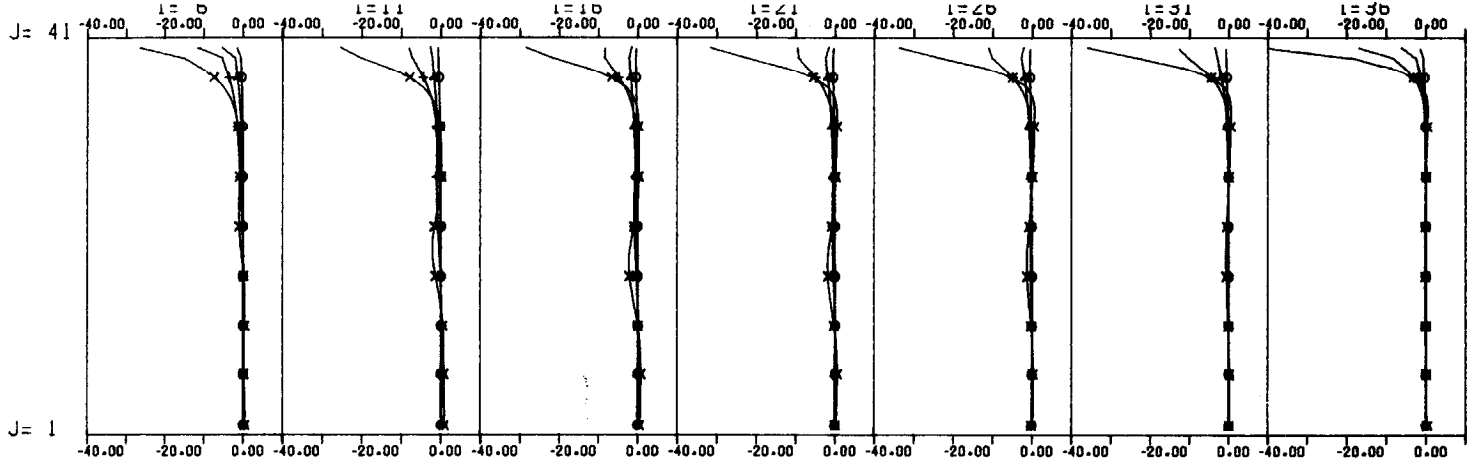

AR=1.000 :⊙ RE=100. :△ RE=400. :+ RE=1000. :× RE=2000.

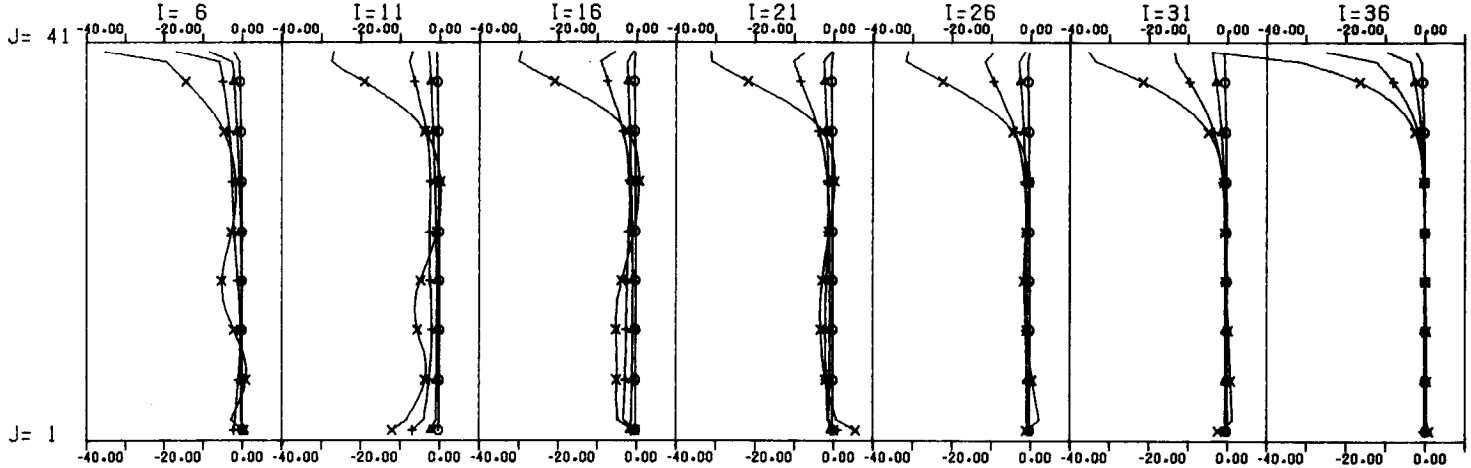

AR=0.500 :⊙ RE=100. :△ RE=400. :+ RE=1000. :× RE=2000.

2. As the Reynolds number is increased, the effect of the inertia terms becomes more dominant. Comparing the flow patterns at the different aspect ratios, there are some apparent differences between large and small aspect ratio. There exist two secondary eddies at large aspect ratio but only one at small aspect ratio. Furthermore, it is found that wind-driven circulation tends to be more stable at a small aspect than at a large one.

3. It is found that the vertical profiles of horizontal velocity bend in the cases $\mathrm{Re} = 2000$ at $\mathrm{AR} = 1.0$ and $\mathrm{AR} = 0.5$. This may be a *symptom of transition* from laminar to turbulent flow. In connection with this, there seems to be a viscous sub-layer near the water surface when the Reynolds number is low. As the Reynolds number is increased, this sub-layer tends to disappear.

APPENDIX

J	Jacobian
ψ	stream function
ζ	vorticity
∇^2	Laplacian
ρ	density of water
ρ_a	density of air
u_*	friction velocity of air
u_s	surface velocity at the midpoint of a cavity
Re	Reynolds number defined in this paper
Re^{B}	Reynolds number defined by Bye [2]
μ	viscosity of water
L	horizontal scale of a cavity
H	vertical scale of a cavity
AR	aspect ratio
ε, ε_n	parameter for convergence
Δx	horizontal size of mesh
Δy	vertical size of mesh
Δt	time interval
P_n	parameter defined as $P_n = 2/\varepsilon_n \Delta t$
X	variable with the limitation of $0 < X \leqslant 1$
Y	variable with the limitation of $0 < Y$
u	horizontal velocity
u''	vertical curvature of horizontal velocity

ACKNOWLEDGMENTS

The author wishes to express his sincere appreciation to Professor H. Charnock for his suggestion and providing the opportunity to study. The author is also grateful to Dr. N. Wells for his good advice and to colleagues of the Department of Oceanography at Southampton University for their stimulating dicussion. These calculations were performed on an ICL 2970 at Southampton University.

REFERENCES

1. K. HIDAKA, *Mem Imperial Marine Obs. Kobe* **7** (1939), 21.
2. J. A. T. BYE, *J. Fluid Mech.* **26** (1966), 577.
3. R. F. WEISS AND B. H. FLORSHEIM, *Phys. Fluids* **8** (1965), 1631.
4. V. O'BRIEN, *Phys. Fluids* **15** (1972), 2089.
5. J. BRANDEIS AND J. ROM, *J. Comput. Phys.* **40** (1981), 396.
6. M. KAWAGUCHI, *J. Phys. Soc. Japan* **16** (1961), 2304.
7. S.-Y. TUANN AND M. D. OLSON, *J. Comput. Phys.* **29** (1978), 1.
8. D. W. PEACEMAN AND H. H. RACHFORD, *J. S.I.A.M.* **3** (1955), 28.
9. C. E. PEARSON, *J. Fluid Mech.* **21** (1965), 611.
10. P. J. ROACHE, "Computational Fluid Dynamics," Hermosa, N.M., 1972.
11. K. MIYAKODA, *J. Meteorol. Soc. Japan* **38** (1960), 107.
12. G. BIRKHOFF, R. S. VARGA, AND D. YOUNG, "Advances in Computers" (F. L. Alt, Ed.), Vol. 3, p. 189, Academic Press, New York, 1962.
13. N. TAKEMATSU, *J. Comput. Phys.* **36** (1980), 236.
14. O. R. BURGGRAF, *J. Fluid Mech.* **24** (1966), 113.
15. G. H. KEULEGAN, *J. Res. Nat. Bur. Stand.* **46** (1951), 358.
16. R. D. MILLS, *J. R. Aeronaut. Soc.* **69** (1965), 116.
17. F. PAN AND A. ACRIVOS, *J. Fluid Mech.* **28** (1967), 643.
18. B. P. LEONARD, "Computer Methods in Fluids" (K. Morgan *et al.*, Eds.), p. 159, Pentech, London/Plymouth, 1980.